*Nigerian Journal of Technology (NIJOTECH)*
*Vol. 39, No. 2, April 2020, pp.* **403 - 416**

Print ISSN: 0331-8443, Electronic ISSN: 2467-8821
www.nijotech.com
http://dx.doi.org/10.4314/njt.v39i2.10

# TRACKING LOCAL BRITTLE ZONE IN THE HEAT AFFECTED ZONE OF GIRTH-WELDED API 5L X46 PIPE

**M. O. H. Amuda[1], L. O. Osoba[2,*], N. N. Etuk[3], T. F. Lawal[4] and A. O. Adetayo[5]**

[1, 2, 3, 4,] MATERIALS DEVELOPMENT AND PROCESSING RESEARCH GROUP (MADEPREG), DEPARTMENT OF METALLURGICAL AND MATERIALS ENGINEERING, UNIVERSITY OF LAGOS, AKOKA, LAGOS STATE, NIGERIA

[5,] MIDWAL ENGINEERING SERVICES LIMITED, 5B ELEGANZA MALL, IKOTA, 101245, LAGOS STATE, NIGERIA

***E-mail addresses:*** [1] *mamuda@unilag.edu.ng,* [2] *losoba@unilag.edu.ng,*
[3] *etuknkerefi2008@yahoo.co.uk,* [4] *wltaiwo@gmail.com,* [5] *adetayo.ayodeji@yahoo.com*

**ABSTRACT**

***In this study, microhardness variation as well as macro and micro structural examination of the heat affected zone (HAZ) of a girth welded API 5L X46 pipeline material were conducted as a means of tracking local brittle zone (LBZ) in the HAZ region. The weldment analysed were built from heat input range of 695 J/mm – 2567 J/mm. Analysis of the results revealed that the HAZ profile changes with variation in the heat input and becomes shallow but wider as the heat input increases. Defects free welds were achieved under the heat input range of 1650 J/mm – 2017 J/mm welding condition. Localized high hardness values were obtained at certain locations within the HAZ of intermediate heat input welds produced at 1467 J/mm due to thermal stresses induced strains at this heat input in the resolidified weld. Other than this, non-equilibrium rapid heating/cooling that is common during welding as well as the magnitude of mechanical strain generated on cooling vary with heat input and was attributed to the development of high hardness value at localized region within the HAZ of the welds in low heat input welding condition. The macrographic profile at these locations, contrasted against that of a failed pipeline material of similar specification obtained from typical oil and gas infrastructure, established that crack initiation and propagation followed the trend of microhardness variations in the girth welded pipe. The crack initiates at specific location in the HAZ with very high hardness in the range 186-216 Hv within a radius of about 3-5 mm from the edge of the fusion zone.***

***Keywords:*** *API 5L X46; Girth welding; Heat input; Heat affected zone; Local brittle zones*

## 1. INTRODUCTION

For many years, researchers pursued the need to develop strong, ductile pipeline material for convenient transportation of pressurized fluid in the oil and gas industry. This led to the design and development of API 5L steel series particularly the X46 for the construction of pipeline infrastructure for oil and gas conveyance [1]. These materials are credited with improved toughness and better microstructural homogeneity than the conventional plain carbon steels of the same composition, which make them suitable and applicable in very hostile on-shore and off-shore environments [2]. Therefore, several tonnages of this steel grade have been used globally in the oil and gas industries especially in the Nigeria's Niger-Delta creek and other parts of the country [3]. Recently, catastrophic failure of the material has been reported resulting in sudden shut down of the entire crude oil conveying system in the Niger-Delta creek. This failure has been attributed in some quarters to vandalism but preliminary field inspection revealed that some of the reported failures are due to rupture in the pipeline network owing to the development of LBZs in the HAZ of the welded API 5L X46 pipeline material. These LBZs are discrete microstructural regions within the HAZ at certain orientation to the weld line which

* Corresponding author, tel: +234 805 426 9424

exhibit significantly lower resistance to fracture than surrounding material. LBZs do manifest in crack initiation and then propagate to the parent plate due to high circumferential pressure externally exerted by the fluid; and consequently, failure occurs. LBZs behaviour is usually associated with initiation by cleavage, but inter-granular fracture has been observed in some instances [4]. Investigations have shown that LBZs in multi-pass welds of API 5L X46 pipeline steels grade can be either in the grain coarsened heat affected zone (GCHAZ) close to the weld fusion boundary or the inter-critically reheated grain coarsened heat affected zone (ICGCHAZ). Although low toughness regions could be present at the boundary between the inter-critical and subcritical heat affected zone (IC/SCHAZ). This is often due to locally intensified strain ageing at a pre-existing crack tip in parent plate, HAZ or weld metal, or within the welds metal itself. But the term is not usually used to describe these cases [5]. LBZs behaviour depends primarily on steel chemistry, welding procedure, welding heat input, and post-weld heat treatment condition [6]. According to BS 7448 [7], the size of a LBZ is a function of welding heat input and the coarsening behaviour of the steel. But, it can be typically, less than 0.5 to 1.0 mm in height and can extend parallel to the weld over a distance of tens of millimetres. The length depends on welding process, weld straightness and frequency of stop/starts. A number of approaches have been adopted by several researchers towards tracking and eliminating LBZs in the HAZ of API 5L steel grade pipeline materials. These include; describing heat inputs condition that needs to be evaluated; modifying the angle of attack between electrodes and the fusion face; modifying weld bead overlap and size to maximize HAZ refinement [8].

Yet, in spite of diligent compliance to all these approaches to track and eliminate LBZs, failures still occur resulting from the presence of LBZs in HAZ which is an indication that the process is not yet optimized. Therefore, additional investigation is deemed necessary to achieve better strategy for tracking LBZs in HAZ of welded API 5L materials particularly the X46 grade. Thus, the current study is a carefully design experimental investigation to track the evolution and manifestation of LBZs within the HAZ with a view to establishing an understanding for the development of a framework to mitigate the development of the phenomena in this girth welded pipeline material.

## 2. MATERIALS AND METHODS

### 2.1 Material

The normalized seamless API 5L X46 pipeline steel grade supplied by Compact Manifold Energy Services (CMES), Marina, Lagos was used in this present investigation. The length of the material pipe was 1500 mm with an inner diameter of 152 mm and 10 mm wall thickness. It can be classified as schedule XS or schedule 80 line pipes according to American Iron and Steel Institute (AISI) schedules for line pipes. Figure 1 shows the image of the seamless as-received API 5L X46 pipeline materials while the chemical composition is presented in Table 1. The carbon equivalent (CE) value was calculated from the relationship proposed by Dearden and O'Neill [9] and adopted by the International Institute for Welding. Additionally, a failed welded API 5L X46 pipe recovered from pipeline network in the Niger-Delta creek of Nigeria was used for validation.

### 2.2 Material Sectioning and Surface Preparation

The as-received API 5L X46 line pipe steel grade of 1500 mm length was sectioned into 18 pieces with each piece having a length of 80 mm using power saw in a cooling medium under a flowing fluid . The surfaces of the sectioned pieces were prepared (bevelled) to create a root, fitted by tag-welding followed by mechanically clamping for girth welding. Figure 2 shows the bevelled and fitted samples.

### 2.3 Welding Process

In order to properly track LBZs in the HAZ of API 5L X46 pipeline material, the fitted samples were manually girth welded using a gas tungsten arc welding (GTAW) in line with the ASME standard WPS for welding of API line pipes.

*Table 1: Chemical composition of the as-received API 5L X46 pipeline material**

| Elemental Composition (wt. %) | | | | | | | | | | |
|---|---|---|---|---|---|---|---|---|---|---|
| C | Si | Mn | P | S | Cr | Ni | Mo | V | Fe | $CE_{IIW}$ |
| 0.194 | 0.184 | 0.652 | 0.02 | 0.003 | 0.12 | 0.043 | 0.037 | 0.194 | 98.3 | 0.376 |

**Analysed at Midwal Engineering Services Lekki, Lagos, Nigeria*

*Figure 1: Image of the as-received API 5L X46 pipeline material*

(a) (b)

*Figure 2: Bevelled and fitted samples (a) bevelled Surfaces (b) fitted samples*

In its basic form, heat input Q (J/mm) delivered during the welding process is dependent on the power of the welding heat source P (W), and welding speed, v (mm/min), through Eqn. (1) [10].

$$Q = \kappa\left(\frac{P}{\upsilon}\right) \quad (1)$$

where $\boldsymbol{k}$ is a constant known as process or efficiency factor. Accordingly, the magnitude of welding heat input can be varied by either changing the power or welding speed. Therefore, welding current and travel speed were varied at three different treatment levels. Table 2 gives a typical ASME standard welding procedure specification (QW-482) as per ASME SECTION IX [11] for welding of API line pipes between X42 and X52 with outside diameter in the range 60.325mm to 323.85mm and wall thickness in the range 5 mm to 19 mm.

However, given that LBZ failures are often produced from prevailing procedure specification, the current study chooses to carry out experimental investigation outside the existing specification. As such, arc current in the range 80 - 140A and travel speed range 72 – 152 mm/min are the modified process parameters employed. Table 3 shows the number of weld joints and the corresponding combinations of process parameters at different levels used in this investigation.

Table 4 gives in details, the number of weld samples, process combination of the welding parameters used and the resulting heat input variation.

GTAW was adopted for both the preliminary passes and the filler and weld cap passes at heat input ranging from 695J/mm to 2567J/mm, corresponding to the ranges of welding current between 80A-140A; and travel speed between 72 mm/min and 152 mm/min. Direct current electrode negative polarity (DCEN) with argon as shielding gas was used for the GTAW. Figure 3 shows the welding process at 6G position and the resulting weld specimens at different welding conditions.

### 2.4 Macro and Microstructural Examination of the Weldments

Macrographs as well as micrographs of the weldments were taken in order to examine the weld and HAZ profile of the API 5L X46 pipeline material weldments at different welding conditions. The samples for metallographic examination were extracted from the weldments and carefully sectioned to achieve a uniform flat surface. Sectioning procedure was carried out in a cooling medium under

a flowing coolant to avoid metallurgical transformations. The sectioned samples were then ground perpendicular to the sectioning direction with emery paper up to 360 grit using Buchler Metaserv 250 grinding/polishing machine. The ground samples were immediately etched with Nitric acid and Ethanol for 30 seconds for macroprofiling. Thereafter, the samples were further ground to 1200 grit surface finish followed by polishing in a combination of diamond and alpha agglomerated alumina pastes for microstructural characterisations preparatory to etching, once again, in a solution of nitric acid and ethanol but for 45 seconds in accordance to ASME SECTION IX (QW-472) [11]. The etched samples were then rinsed in water and then dried with a blast of warm air. The macroprofile of the samples were viewed using a Leica's stereographic microscope model M50 whilst microstructural characterisations were conducted using a CETI 0703552 metallurgical microscope.

### 2.5 Microhardness Profiling

In this investigation, Vickers microhardness survey was conducted under the applied load of 5 kgf for 10 seconds using automated microhardness tester (Innova test Falcon 500), in accordance to ASTM E384 standard test method. The Microhardness survey was conducted at 0.5 mm across and 2 mm along the transverse and longitudinal sections on all samples extracted from each of the API 5L X46 welds. The test was repeated thrice and the average taken as the representative value. Given that LBZs are produced at particular orientation to the weld line, the microhardness survey was aimed at profiling LBZs at transverse, longitudinal and 45° locations within the fusion zone and HAZ of the API 5L X46 welds. Figure 4 presents the image acquisition of specimens for microhardness survey extracted from the parent weld.

The schematic illustration of the acquisitions of the microhardness survey across both the transverse and longitudinal sections is shown in Figure 5a while Figure 5b presents the impression of the microhardness indentations on the welds across both sections of the welds as well as about 45° inclination within the HAZ.

### 2.6 Tensile Strength Profiling

Samples for tensile testing were sectioned from the as-received API 5L X46 material as well as from the welded region. Tensile testing was equally conducted thrice on an Instron machine rated 100 KN at a strain rate of $2 \times 10\text{-}3s^{-1}$ at room temperature in accordance with ASTM E8/E8M Standard [12]2018) complemented with API STD 1104 [13] in Figure 6.

## 3. RESULTS AND DISCUSION

### 3.1 Visual Inspection and Macrostuctural Analysis of A Failed API 5L X46 Pipeline Material

Figure 7 is the fracture profile obtained from a failed 305 mm diameter API 5L X46 pipeline material excavated from a crude oil delivery line in the Niger Delta creek of Nigeria. The image acquisition in Figure 7a shows the progression of fracture path along the axial length rather than circumferential direction of the pipe. This suggests that the failure was not around the fusion zone (FZ) but within the region of the HAZ in a circumferential joint. If the failure were to be within the FZ, the crack opening would have propagated in the circumferential direction. Linear measurement of the sectioned region of the failed pipeline material containing the fracture region (Figure 7b) indicates a longitudinal fracture length of about 275 mm.

The figure further revealed that the fracture proceeded from one end of the pipe and tapered off at about 25 mm. The maximum width of the fracture opening is 25.16 mm located at one end of the pipe (see the arrow in Figure 7b). An examination of the crack propagation trajectory in Figure 7(c) reveals a widened flat fracture surface in the span of section A which progressively closes up at Section B and almost ease out at Section C.

*Table 2: ASME standard WPS for welding of API line pipes between X42 and X52*

| No. of passes | Filler/Electrode | Rod diameter (mm) | DC Current (A) | Voltage (V) | Travel speed (mm/min) |
|---|---|---|---|---|---|
| Root | E-6010/E7018 | 1/8" (3.2mm) | 70-100 | 18-26 | 100-250 |
| Hot | E-6010/E7018 | 5/32" (4mm) | 125-132 | 18-26 | 152-305 |
| Filler | E-6010/E7018 | 5/32" (4mm) | 125-132 | 18-26 | 200-330 |
| Cap | E-6010/E7018 | 5/32" (4mm) | 125-132 | 18-26 | 200-330 |

***ASME Welding Standard Manual Vol.3 welding procedure specifications [11])*

*Table 3: Welding variables and their treatment levels*

| Number Weld Joints (N) | Welding Current (Amps) | Travel Speed (mm/min) |
|---|---|---|
| 1 | 80 | 72 |
| 2 | 80 | 112 |
| 3 | 80 | 152 |
| 4 | 110 | 72 |
| 5 | 110 | 112 |
| 6 | 110 | 152 |
| 7 | 140 | 72 |
| 8 | 140 | 112 |
| 9 | 140 | 152 |

*Table 4: Process parameters combination and heat inputs (with k =60)*

| Welding Samples | Welding Current (Amps) | Travel Speed (mm/min) | Arc Voltage (Volts) | Heat Input (J/mm) |
|---|---|---|---|---|
| Sample A | 80 | 72 | 22 | 1467 (M) |
| Sample B | 80 | 112 | 22 | 943 (L) |
| Sample C | 80 | 152 | 22 | 695 (L) |
| Sample D | 110 | 72 | 22 | 2017 (H) |
| Sample E | 110 | 112 | 22 | 1296 (M) |
| Sample F | 110 | 152 | 22 | 955.3(L) |
| Sample G | 140 | 72 | 22 | 2567 (H) |
| Sample H | 140 | 112 | 22 | 1650 (H) |
| Sample I | 140 | 152 | 22 | 1216 (M) |

*L = low level; M = mid-point or intermediate level; H = high level*


*Figure 3: Gas tungsten arc welding process: (a) welding of specimens at 6G position and (b) weld specimens*

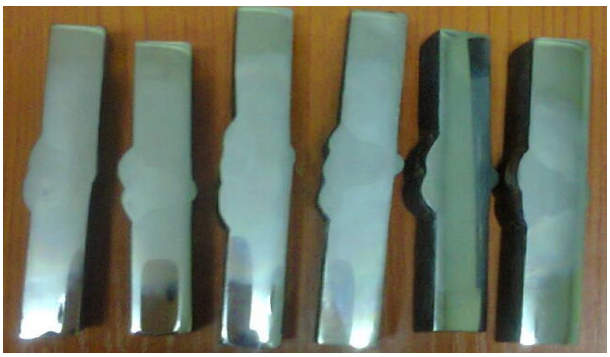

*Figure 4: Image acquisition of specimens extracted from the weldments for microhardness profiling*

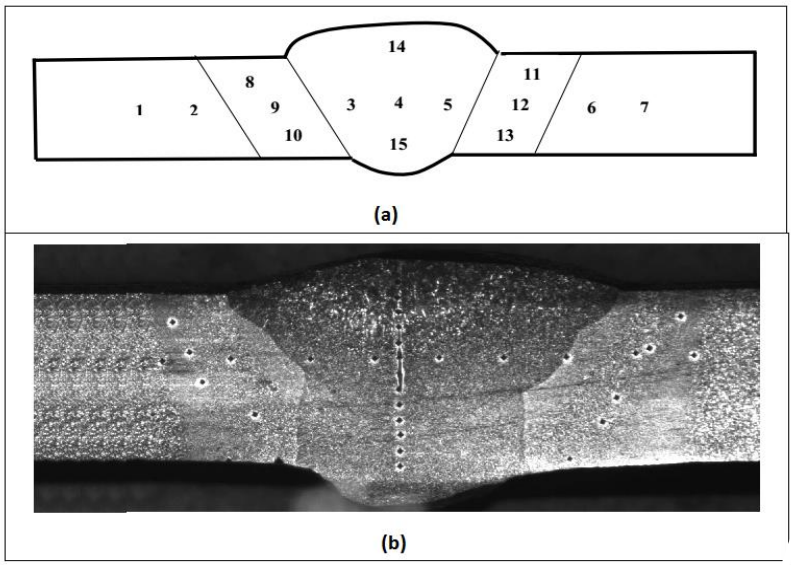


Indentation at 45$^{O}$ to the weld line

*Figure 5: Illustration of microhardness indentation positions on the API 5L X46 girth welds: (a) schematic illustration and (b) image presentation of actual indentation positions*

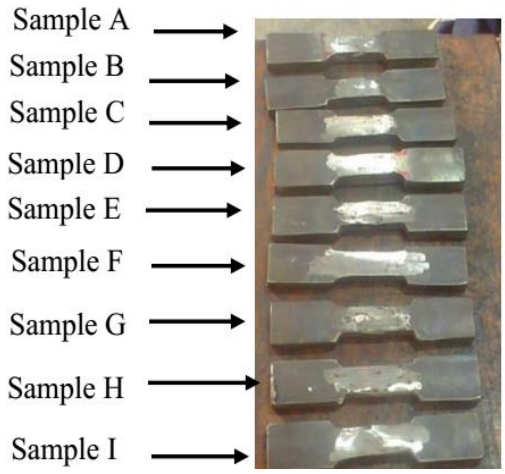


*Figure 6: Tensile test specimens extracted from API 5L X46 weld coupons*

This implies that crack propagation is rapid in Section A and slows down around and beyond Section B. Crack dynamics of this nature approximate brittle fracture consistent with fatigue loading.

Further validation of Section A via the evaluation of the microhardness of the region shown in Figure 8 established the presence of points within the HAZ exhibiting a sharp increase in microhardness values in the range 250 – 325 HV unlike the average value of 225 HV in the weld metal (FZ). These points are between 2.5 mm and 3.5 mm from the FZ.

### 3.2 Analysis of Macroprofiles of Weld Coupons

The macrographs showing the weld profiles of the coupons produced at different heat inputs using GTAW are presented in Figure 9 .The range of heat input investigated was divided into three classifications and these are: heat input in the range 695J/mm-955.3J/mm(less than 1000 J/mm as low heat input, those greater than 1000 J/mm but less than 1500 J/mm (1216J/mm-1467J/mm) is classified as intermediate heat input and those greater than 1500 J/mm (1650J/mm-2567J/mm) are classified as high heat input. The macrographs revealed that the HAZ profile is affected by changes in the heat input. In specifics, as the heat input changed from low to medium and high heat input, the weld profile assumed a shallow depth in the thickness direction with a large surface width in addition to a progressively widened HAZ region (see Figure 9a-c). The trend of the weld profile with change in heat input is similar to previously reported work by Richards et al. [14]. Though, the size of the HAZ increases as the heat input transits from low to intermediate and high heat inputs but the depth of penetration significantly becomes shorter. Indeed, for the intermediate and high heat input weld coupons, a prior root cap was deposited for full weld penetration to be accomplished (see Figure 9b and 9c). Thus, low heat input appears to deliver better weld shape and size in terms of width, penetration depth and minimal geometrical distortion in the welded coupons.

### 3.3 Microstructural Analysis of Weld Coupons

The microstructure of the as-received API 5L X46 pipeline steel grade shown in Figure 10 consists of ferrite matrix and dark patches of pearlite.

Microstructural analyses of the weld coupons produced at different heat inputs could be used to evaluate the influence of heat input on microstructural inhomogeneity in the welds which facilitates the development of LBZs in the HAZ. The micrographs of the welds at various heat inputs shown in Figure 11-13 clearly reveal the change in grain morphology in relation to the heat input. Also, some phase transformation products were also observed. For weld coupons at low heat input (less than 1000 J/mm, see Figure 11), the microstructure in this condition indicates the formation of equiaxed ferrite matrix in the FZ and carbides at the HAZ. The typical elongated columnar structure often obtained in fusion welds was absent under this condition. This suggests that the development of columnar structure in fusion welds may after all be a function of the level of the heat input. Other microstructural features equaly observed under this condition of heat input include grain boundary ferrite (GBF) and grain boundary maternsite (GBM) (see Figure 11 b and c).

Figure 12 shows the microstructures of weld coupons produced at intermediate heat input (less than 1500 J/mm). The change in grain structure within the intermediate heat input in both the FZ and HAZ is not quite apparent suggetsing that the thermal conditions within this heat input range is almost the same. But unlike the equiaxed grain structure in the low heat input welds, the grain structure in this condition is esentially columnar (see Figure 12) across the FZ but more of equiaxed in the HAZ particulalry in the region adjacent to the FZ line. But at the upper band of the intermediate heat input (1467 J/mm), small amount of large ferrite grains and GBM were present (see Figure 12c).

Microstructures of weld produced at high heat input greater than 1500 J/mm are presented in Figure 13. The microstucture of weld produced at heat input of 1650 J/mm (Figure 13a) revealed the formation of acicular ferrite (AF) grain structure. The microstructure in the welds produced at heat input of 2017 J/mm and 2567 J/mm revealed the formation of equiaxed grain structures and grain boundary ferrites in the FZs whereas columnar ferrites grains were observed in the HAZ. These grain boundary ferrites could be detrimental to the weld coupons. AF observed in Figure 13a is a structural phase of ferrite in steel that is characterised by needle-shaped crystallites or grains when viewed in two dimensions. This phase is generally found to be positive for weld strength and impact toughness [14]. This is accountable for the high yield strength recorded from the weld during tension test. At higher heat input rate, microstructural features such as coarse ferrite grains were also observed. This suggests that at high heat input, the cooling rate is slow with transformation of austenite (γ) to α-ferrite.

### 3.4 Analysis of Mechanical Properties of Weld Coupons

#### *3.4.1 Microhardness Profiling in the Weld Specimens*

Microhardness survey was performed across the FZ and the HAZ of grit welded coupons produced at different heat input conditions. The survey was used to track LBZs in the HAZ of the material through comparative analyses of the microhardness at various regions. The locations both schematic and real time indentation in which the microhardness survey was carried out across the weld shown in Figure 5 provide the total number of indentations acquired in relation to the traverse and longitudinal directions. .

The microhardness profiles of resolidified welds in longitudinal direction are presented in Figure 14. The figure revealed that the microhardness values in the resolidified weld follows a sinusoidal behaviour in the longitudinal directions across all heat inputs revealing the significance of welding heat input on the parameter. It is higher at the weld centre line in the FZ and decreases onwards to the HAZ with a further increase from the HAZ to the base metal generating a periodical behaviour. Peak values in microhardness are displayed at the weld center as well as at a distance 6 mm to both left and right of weld center line. This trend suggests the generation of cyclic thermal strains in the weld initiating from the FZ to the HAZ and then to the base metal. The thermal strains must have resulted from thermal stresses induced during welding and their magnitude is dependent on allowable heat input.

The specific microhardness profiles observed in the longitudinal direction is further accentuated by the heat input. For instance, coupons welded with intermediate heat input of 1467 J/mm exhibits the highest microhardness value of 219HV across the indentation points unlike those welded at low heat input of 955.3 J/mm and the high heat input of 2567 J/mm.

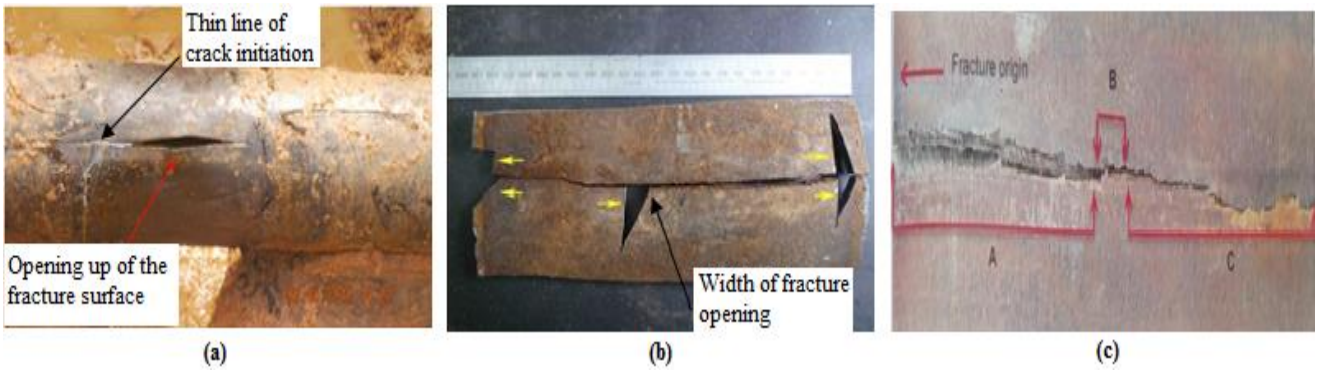


*Figure 7: Images and macroprofile of a failed 305 mm API 5L X46 pipeline material: (a) as-received failed material, (b) crack trajectory in the failed material and (c) magnified sectional view of crack propagation in the failed material*

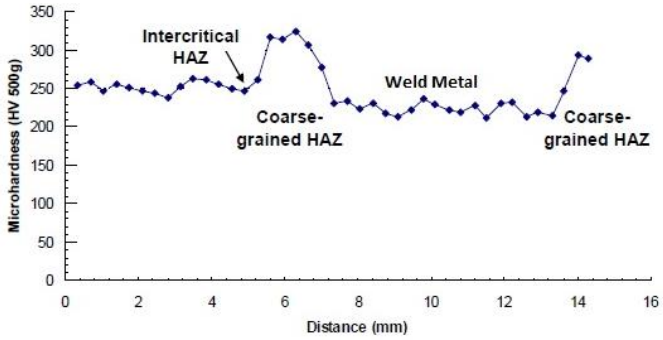


*Figure 8: Hardness trend along Section A (Figure 6c) highlighting points of localised sharp hardness values*

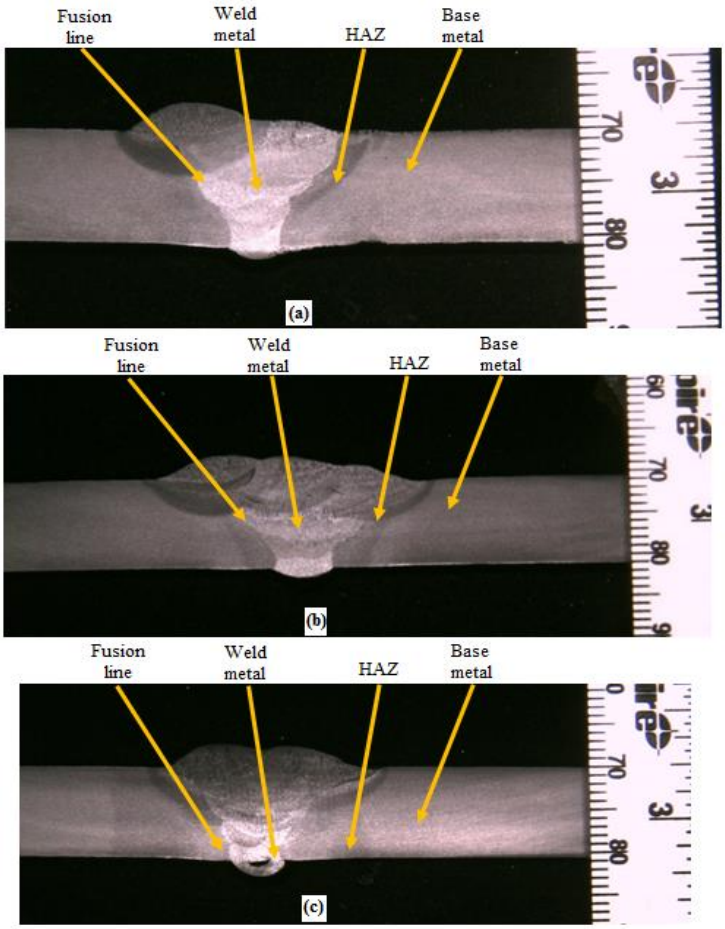


*Figure 9: Macroprofile API 5L X46 weld coupons at different ranges of heat input: (a) low heat input, (b) intermediate heat input and (c) high heat input*

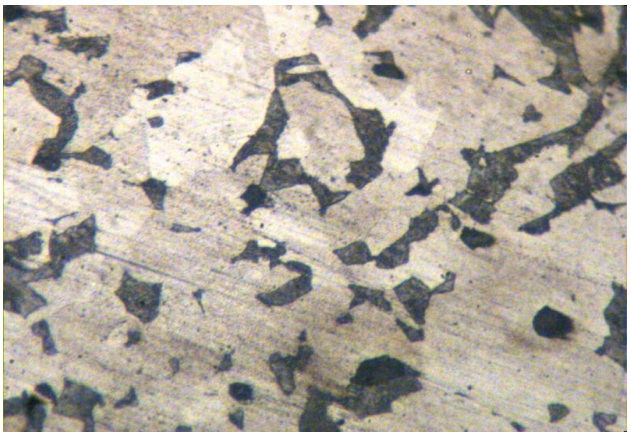

*Figure 10: Micrograph of as-received API 5L X46 material showing ferritic matrix background and dark patches of pearlite*

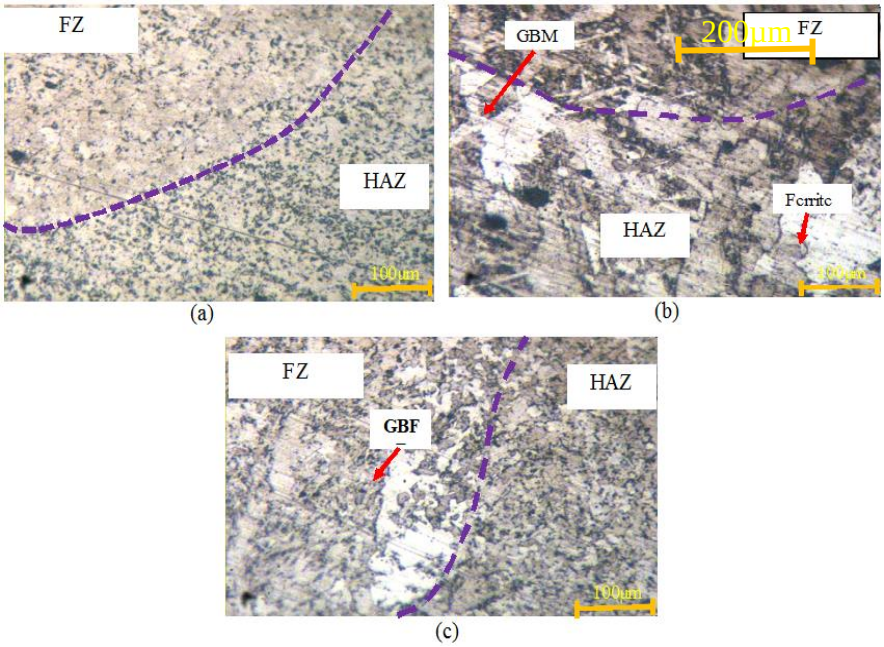


*Figure 11: Micrographs of weld coupons at ranges of low heat input less than 1000 J/mm: (a) 695 J/mm, (b) 943 J/mm and (c) 955 J/mm*

The spots of exceptional high microhardness value are essentially within the HAZ and appear to approximate the region within the coarse grain HAZ shown in Figure 7 which was obtained from a failed API pipeline material of the same composition as the welded coupons. The trend in the microhardness values in both the FZ and HAZ in the longitudinal direction could be attributed to microstructural transformation and the stress-strain dynamics in the coupons resulting in the formation of martensite during the resolidification of the welds.

Figure 15 presents the microhardness profiles of the resolidified welds in the transverse direction. Whilst the trend is different from that in the longitudinal direction, it is equally dictated by the welding heat input. For welds produced at low heat input, the microhardness value remain almost constant until at a depth of 1.5 mm beyond which it increased with depth of penetration. In welds produced at intermediate heat input, marginal increase in microhardness value was obtained until at a depth of about 1.8 mm where a progressive decrease in microhardness was obtained. Whereas in the welds produced with high heat input, progressive decrease in the microhardness value was obtained across the depth of the welds. A maximum microhardness value of 230 HV was obtained in welds produced with low heat input at a depth of 3.0 mm which is higher than the maximum microhardness value obtainable from either intermediate or high input condition. The peak value in intermediate heat input welds is about 220 HV at a depth of 0.5 mm and in high input welds,

the value is about 207 HV at a depth of 0.5 mm. This trend of microhardness in the transverse direction is attributable to differential cooling rate in the thickness direction due to the varying heat input.

Microhardness behaviour at 45° left and right to the weld centreline is shown in Figure 16. The figure shows that the trend is similar to that in the transverse direction at low heat input condition (955. 3 J/mm). Since the 45° orientation is within the HAZ, the trend in the microhardness characteristics in the welded coupons confirms that spots of high hardness value are restricted within the HAZ. This is suggestive that LBZs are essentially HAZ phenomenon. These spots are about 2 mm from the weld centre line both from the left and right (See Figure 16a and b) irrespective of the heat input.

The high microhardness variation in the longitudinal and transverse direction of the welded coupons can be considered as LBZs. This is reinforced with the trend in Figure 16. The phenomenon of LBZs have been previously attributed by Funderburk [15] to be due to the occurrence of rapid cooling at low heat input welding condition, while, Bhadeshia [16] indicated that LBZs are general practical problem associated with welding of carbon steel pipes. Similarly, previous work on weld cracking in IN 718 superalloys [17] have shown that cracking generally occurs when significant amounts of thermal strains are generated during weld cooling particularly in low heat input conditions.

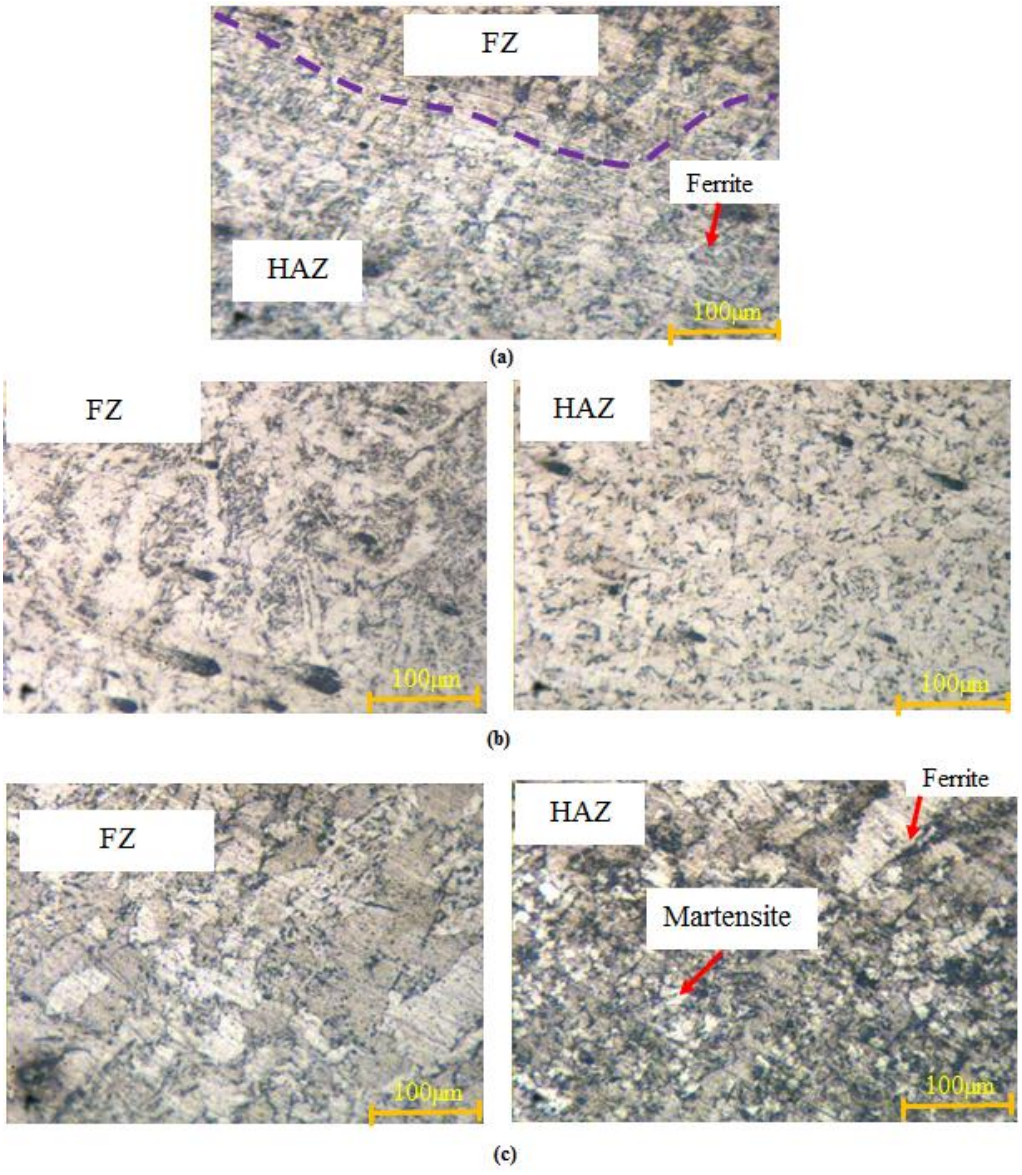


*Figure 12: Micrographs of weld coupons at ranges of intermediate heat input less than 1500J/mm: (a) 1216 J/mm, (b) 1296 J/mm and (c) 1467 J/mm*

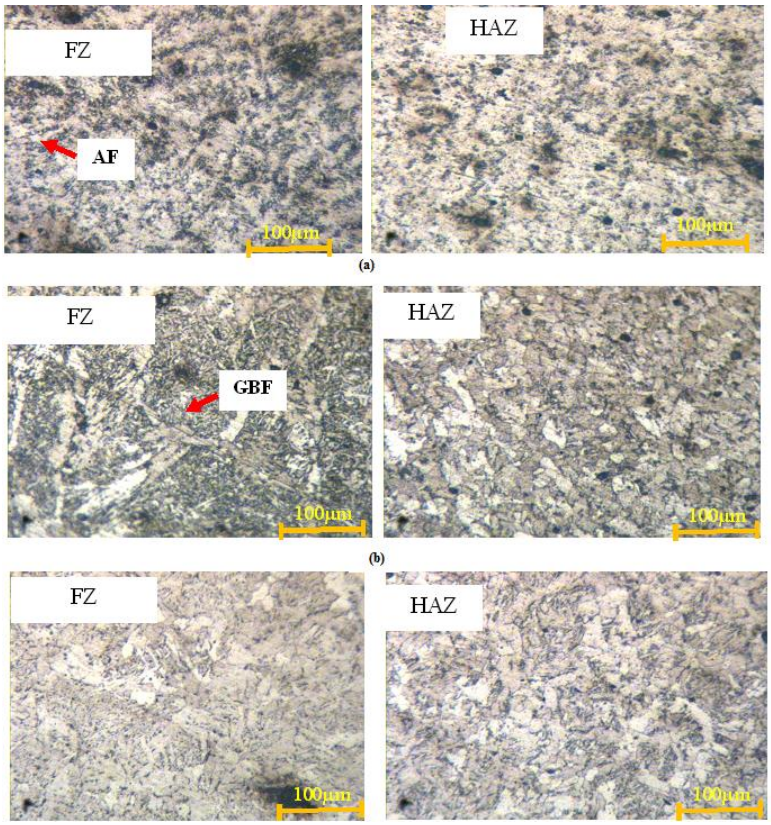


*Figure 13: Micrographs of weld coupons at ranges of high heat input: (a) 1650 J/mm, (b) 2017 J/mm and (c) 2567 J/mm*

Though, the differential cooling rates associated with the present work has not been evaluated but the work of Bhadeshia [16] appear to suggest that LBZs are consequential effect in the welding of ferrous pipes. Yet, what the present work has demonstrated is that spots of occasional high hardness may be used as an indicator of the likelihood of the presence of LBZs particularly in the regions of the HAZ adjacent to the weld interface.

### *3.4.2 Analysis of Weld Tensile Strength*

Figure 17 shows the stress-strain distribution in as-received materials during tension testing for material verification. The yield and tensile strength of the material are 450 MPa and 650 MPa, respectively. These values are within the range specify for API 5L X46 steel grade for Product Specification Level 2 (PSL2) [18]. However, the trend of these strength in the welded coupons across the heat inputs is shown in Figure 18. The figure shows that welding process parameters have less significant effect on the tensile strength unlike the yield strength.

The after-weld tensile strength in the coupons averaged 551 MPa relative to 650MPa in the as-received base metal. However, the yield strength is significantly affected by the heat input. The yield strength progressively decreases with increasing heat input in the low heat input range (695-955 J/mm) and maintains a plateau at the intermediate heat input range (1216-1467 J/mm) beyond which it rises with increasing heat input in the higher heat input range increases (1650 -2567 J/mm). In the range of heat input considered in the present investigation, the yield strength decreased from 450 MPa in the as-received base metal to about 331 MPa in the welded coupons. The trend in the profile of the yield strength in Figure 18 approximates the behaviour observed in the crack initiation and propagation trajectory shown in Figure 7. The trajectory suggests a higher stress level for crack initiation and a reduced stress level for propagation particularly in the low heat input range. This is indicative of ductile flow in the crack initiation before transiting to a possible brittle fracture which is accentuated by a combination of environmental condition and the flow regime of the pressurised fluid in the pipeline material.

Therefore, the development of isolated spots of high hardness value (LBZ) as obtained in the HAZ is considered to have influenced the behaviour of the welded coupons at different heat inputs particularly at the intermediate heat input range. In specifics, heat input in the range 1216 J/mm – 1650 J/mm

generated lower yield strengths and could support failure from brittle fracture relative to other process parameter combination.

The fracture locations in the various welds during tension testing are shown in Table 5. The table indicates that within the range of process parameter considered in the present work, most of the fracture points are located in the weld; only few are in the base metal. Even at that, the fracture often occurred at the interface between the HAZ and the base metal. While fracturing at the weld metal zone can be attributed to the presence of as-cast structure in the weld those outside the weld metal could be attributed to the presence of spots with outside-the-range hardness values. These points are considered to be the LBZs. Microhardness characterisations reveal that these points are about 3-6 mm from the weld interface or into the HAZ.

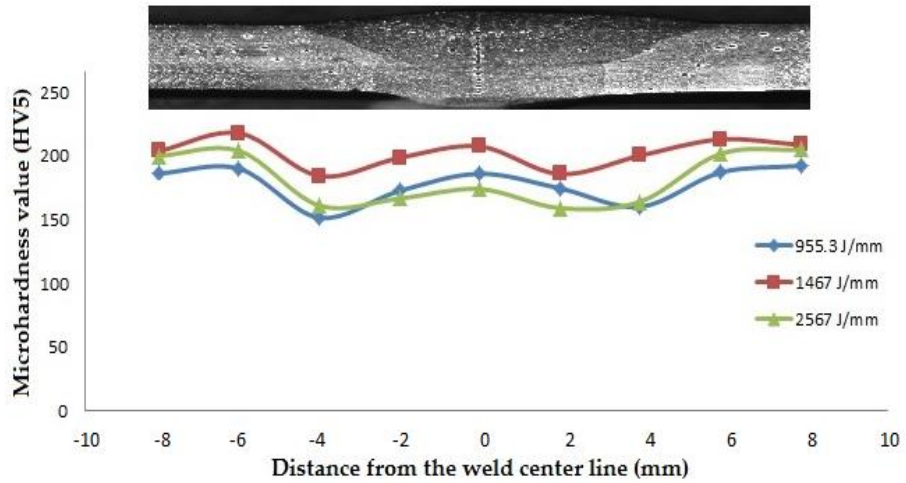


*Figure 14: Longitudinal microhardness profiles of the grit welds produced at varying heat input*

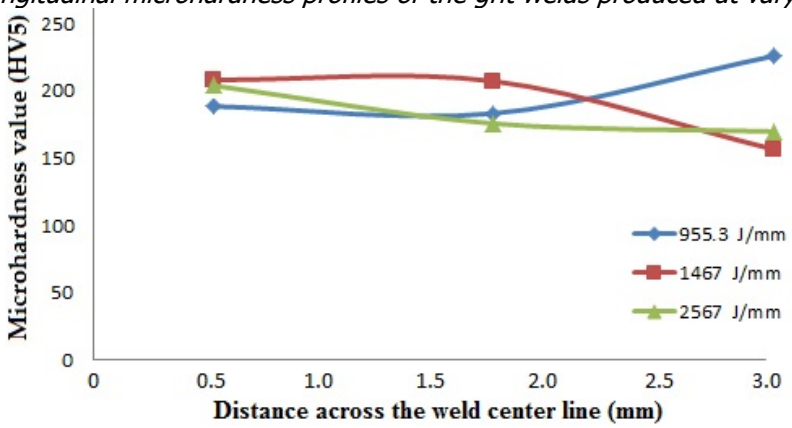


*Figure 15: Transverse microhardness profile of the grit welds produced at varying heat input.*

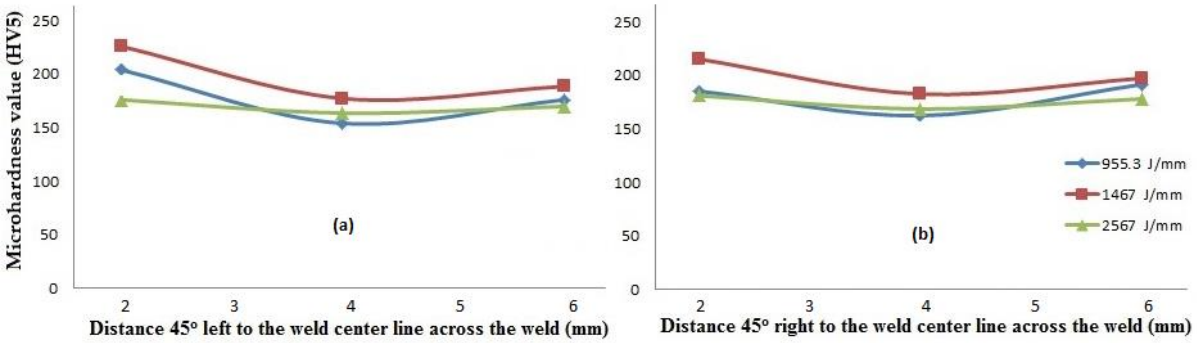


*Figure 16: HAZ microhardness profiles of the grit welds produced at varying heat input: (a)* 45° left of weld center (b) 45° right of center line

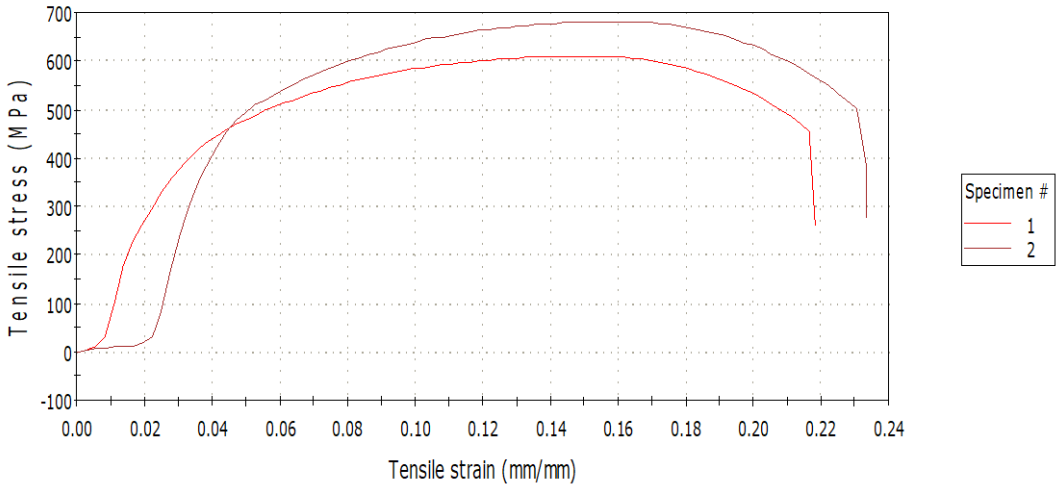


*Figure 17: Tensile behaviour in as-received API 5L X46 pipeline material*

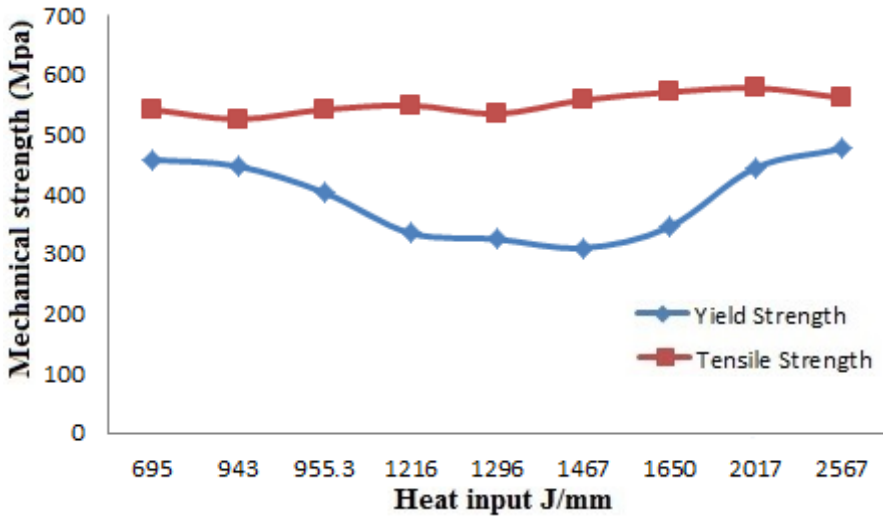


*Figure 18: Yield and tensile strengths of welds produced at different heat inputs*

*Table 5: Fracture points locations in welded coupons produced at different process parameters*

| Samples | Current (A) | Welding Speed (mm/min) | Heat Input (J/mm) | Fracture Location |
|---|---|---|---|---|
| A | 80 | 72 | 1467 | Failure in weld metal |
| B | 80 | 112 | 943 | Failure in weld metal |
| C | 80 | 152 | 695 | Failure in weld metal |
| D | 110 | 72 | 2017 | Failure in base metal |
| E | 110 | 112 | 1296 | Failure in base metal |
| F | 110 | 152 | 955.3 | Failure in weld metal |
| G | 140 | 72 | 2567 | Failure in weld metal |
| H | 140 | 112 | 1650 | Failure in base metal |
| I | 140 | 152 | 1216 | Failure in base metal |

## 4. CONCLUSION

Microhardness variations in welded API 5L X46 pipeline material produced at varying welding conditions have been studied to track LBZs in the HAZ of API 5L X46 pipeline materials and the following conclusions emerged:

1. The range of process parameters used in the present work successfully produced defect free welds with mechanical properties within

acceptable range as specified in standard reference.

2. The development of LBZs in the welded coupons is characterised by localised elevated microhardness values in some locations within the HAZ close to the weld interface and such spots are common in weld produced with low heat input.
3. Process parameters combination involving welding current ranging from 80A-140A and travel speed ranging from 72 mm/min – 152 mm/min has minimal effect on the development of LBZs within the HAZ of API 5L X46 welds.

## 5. ACKNOWLEDGEMENT

This work is supported by the Central Research Committee of the University of Lagos, Nigeria under Grant No: CRC M2015/05**.** The President, management and technical staff of Midwal Engineering Services Limited, Lekki-Ajah, Lagos, Nigeria for providing technical support during macroprofiling of the weld coupons.

## 6. REFERENCES

[1] American Petroleum Institute . *API 5L specification for line pipes*, American Petroleum Institute, 1220 L Street, N.W., Washington, D.C. 20005, 2004.

[2] Beltran, M.A, Gonzalez, J.L, Rivas, D., Hernandez, F. and Dorantes, H. "On the role of microstructural properties on mechanical behaviour of API-X46 steel" *Procedia Structural Integrity*, Vol.16, 2017, pp 57-67.

[3] Tinsley, R. D. *Natural gas pipeline and storage infrastructure projections through 2030*, The INGAA Foundation Inc. Washington DC 20002, 2000.

[4] Kim, S. "Effect of alloying elements on fracture toughness in the transition temperature region of base metals and simulated heat affected zones of Mn-Mo-Ni low alloy steels", *Metallurgical and Materials transaction A,* Vol. 35 Issue 7, 2004, pp 2029-2031.

[5] Barness, A. M. *Local brittle zones in C-Mn Steel multipass welds,* The Welding Institute Bulletin. The Welding Institute, Cambridge, UK, 1990.

[6] BS 7910 .*Guide to methods for assessing the acceptability of flaws in metallic structures*, Paperback by British Standards Institution, (ISBN-10:0580601080), London, UK, 2005

[7] BS 7448. *Fracture mechanics toughness tests: Method for determination of fracture resistance curves and initiation values for stable crack extension in metallic materials,* British Standard Institution. London, UK, 1997

[8] API RP 2Z. *Recommended practice for preproduction qualification for steel plates for offshore structures,* Fourth edition. American Petroleum Institute. Washington DC, 2005.

[9] Dearden, J. and O'Neill, H. "A guide to the selection and welding of low alloy structural steels", *Transactions of the Institute of Welding,* Vol. 3, 1940, pp 203-214.

[10] Melfi, T. "New codes requirement for calculating heat input", *Welding Jounal*, Vol. 6, 2010, pp 61-69.

[11] ASME SECTION IX . *Rules for construction of power boilers,* The American Society of Mechanical Engineers. Three Park Avenue, New York, NY 10016-5990, 2011.

[12] ASTM E8/E8M. *Standard test methods for tension testing of metallic materials*. ASTM International, Pennsylvania. 2013.

[13] API STD 1104. *Welding of pipelines and related facilities*. 21st edition, American Petroleum Institute, Washington. 2013.

[14] Richards N.L, Nakkalil, R and Chaturvedi, M. C . "The Influence of EBW parameters on HAZ microfissuring in Incoloy 903", *Metallurgical and Materials Transactions A*, Vol. 25A, 1994, pp 1733-1743.

[15] Funderburk, R. S. "Key concepts in welding engineering", *Welding Innovation,* Vol.16, Issue 1, 1999, pp 1-4.

[16] Bhadeshia, H. K. D. H. *Local brittle zones and the role of niobium,* University of Cambridge, Materials Science and Metallurgy U. K, 2014.

[17] Osoba, L.O, Zhiquo, G. and Ojo, O. A. "Heat input dependence of weld HAZ cracking in aerospace superalloy Haynes 282", *In Proceedings of The Canadian Society for Mechanical Engineering International Congress*, 2012.

[18] Sharma, S. K. and Maheshwari, S. "A review on welding of high strength oil and gas pipeline steels", *Journal of Natural Gas Science and Engineering,* Vol. 38, 2017, pp 203-217.